Journal of Nanoparticle Research (2005) 7: 249–263
DOI: 10.1007/s11051-005-4717-9

Preparation of nanosized iron oxide and its application in low temperature CO oxidation

Hsin-Yu Lin[1], Yu-Wen Chen[1] and Wei-Jye Wang[2]
[1]*Department of Chemical and Materials Engineering, Nanocatalysis Research Center, National Central University, Chung-Li 320, Taiwan, ROC (Fax: +886-3-4252296; E-mail: ywchen@cc.ncu.edu.tw);*
[2]*Department of Chemical Engineering, Far-East College, 744 Shin-Shih, Taiwan, ROC*

Received 28 November 2004; accepted in revised form 29 March 2005

Key words: iron oxide, CO oxidation, nanoparticle, gas mask, catalysts, aerosols

Abstract

A method to prepare iron oxide material which has a higher surface area and nanosized particle was developed. It was used as a catalyst for CO oxidation at low temperature. Iron oxide materials were prepared by precipitation under constant pH value. The effects of preparation parameters, such as iron salt ($FeCl_3$, $Fe(NO_3)_3$ and $FeCl_2$), pH value (between 8 and 12), drying temperature (between 120°C and 300°C), and feeding rate of the aqueous solution of the iron salt, on the characteristics of iron oxide have been investigated. The materials were characterized by N_2 sorption, powder X-ray diffraction (XRD), transmission electron microscopy (TEM) and X-ray photoelectron spectroscopy (XPS). The surface area of iron oxide was greater than 400 m^2/g using $FeCl_3$ as the starting material with very low feeding rate of 10 ml/min, the pH value of 11, and drying at 120°C. The XRD patterns indicated that the iron oxide samples heated at a temperature below 180°C was either amorphous or of a particle size too small (< 4 nm) for the samples prepared with $FeCl_3$. Depending on the preparation conditions, the iron oxide samples showed a phase transition from amorphous to various crystalline phases. Large amount of hydroxyl groups were preserved if the drying temperature was below 200°C. TEM images showed that the particle diameters were less than 4 nm for the samples prepared with $FeCl_3$ at pH value of 11 with a low feeding rate of 10 ml/min, and heated below 200°C. XPS Fe $2p_{3/2}$ spectra showed the phase transition of iron oxide from Fe_3O_4 to FeO. The feeding rate of starting material and pH value during precipitation played the important roles to obtain iron oxide with high surface area. The nanosized iron oxide demonstrated high activity for CO oxidation even at ambient condition. The higher activity of Fe_xO_y nanoparticles in CO oxidation was attributed to a small particle size, high surface area, high concentration of hydroxyl groups, and more densely populated surface coordination unsaturated sites.

Introduction

The oxidation of CO is one of the simplest reactions. It covers a wide range of applications from gas masks, rescue equipment, gas sensors, regenerative CO_2 lasers, indoor air quality control to hydrogen purification for polymer electrolyte fuel cells. Transition metal oxides are less costly alternatives to the precious metals-based catalysts for carbon monoxide oxidation. Nanophase transition metal oxides, with small particle size, high surface area, and perhaps, more densely populated surface coordination unsaturated sites, could potentially improve catalytic activity over non-nano oxide catalysts. Iron oxide has been reported to be a good support for gold catalysts in CO oxidation at low

temperature (Bond & Thompson, 1999; Kozlova et al., 1999; Tabakova et al., 2000; Avgouropoulos et al., 2002; Cameron et al., 2003; Haruta, 2004; Wu et al., 2004). However, gold is very expensive. Nanosized iron oxide itself has also been reported to be a good catalyst for CO oxidation (Li et al., 2003) and direct coal liquefaction (Feng et al., 1993; Huffman et al., 1993; Zhao et al., 1993). However, it was used at high temperature (> 250°C), instead of room temperature. Li et al. (2003) reported the higher activity of Fe_2O_3 nanoparticles over non-nano Fe_2O_3 powders for CO oxidation only at temperature avove 210°C. It was attributed to a small size (3 nm) and the presence of a hydroxylated phase of iron oxide (FeOOH). However, iron oxide nanoparticles are only active at 300°C. Kozlova et al. (1998) used $Fe(NO_3)_3$ and Na_2CO_3 to prepare the iron oxide samples. $Fe(NO_3)_3$ was added dropwisely (8 ml/min) to an aqueous solution of Na_2CO_3 under vigorous stirring. Final pH of the mixture was ca. 9.1. The iron oxide was active for CO oxidation only at temperature higher than 190°C. Neri et al. (1999) prepared iron oxide samples by addition of a solution of $Fe(NO_3)_3$ to an aqueous solution of Na_2CO_3 1 M (pH 11.9) or NaOH 1 M (pH 14) under vigorous stirring (500 rpm) at 7.5 ml/min rate and at temperature at 273 and 348 K. The highest surface area they got was 195 m^2/g. Venugopal and Scurrell used $Fe(NO_3)_3$ and NH_4OH to prepare iron hydroxide. The highest surface area they obtained was 54 m^2/g. The literature did not show any iron oxide which was active at temperature below 200°C for CO oxidation (Venugopal & Scurrell, 2004).

If the nanosized iron hydroxide is prepared, providing large active surface area, and whole bulk material is in hydroxide structure, i.e., large amount of hydroxyl groups are present, instead of only surface FeOOH species, this material will be very active in CO oxidation. The aim of this research was to develop a nanosized iron hydroxide catalyst which is active even at ambient condition. A method to prepare iron oxide material which has a higher surface area and nanosized particle was developed in this study. It was test as a catalyst for CO oxidation at ambient temperature. The material was prepared by precipitation method. The effects of preparation parameters, such as iron salt ($FeCl_3$, $Fe(NO_3)_3$ and $FeCl_2$), pH value (from 8 to 12), drying temperature (from 120°C to 300°C), and feeding rate of iron precursor on the properties of iron oxide materials have been investigated. The iron oxide was characterized by N_2 sorption, powder X-ray diffraction (XRD), transmission electron microscopy (TEM) and X-ray photoelectron spectroscopy (XPS). The CO oxidation reaction was carried out in the presence of moisture at room temperature.

Experimental

Chemical

Reagents used were analytical grade without further pretreatment. $Fe(NO_3)_3{\cdot}9H_2O$, $FeCl_2{\cdot}4H_2O$, $FeCl_3{\cdot}6H_2O$ and NH_4OH (Showa, Japan) were used as the starting materials for preparation of the Fe_xO_y support.

Catalyst preparation

Iron oxide was prepared by precipitation method. In typical procedure, an aqueous solution of iron salt (0.1 mol in 200 ml H_2O) was added dropwisely (10 ml/min) to an aqueous solution of NH_4OH (15%) under vigorous stirring. These two solutions were slowly added to a container. The flow rates of these two solutions were regulated to have constant pH value in the mixed solution. Various flow rates of the iron salt solution and various pH values in the mixed solution were tested in this study. The pH of the mixture was maintained at a fixed value in the range between 7 and 12. After aging at room temperature for 2 h, the brown precipitate was filtered and washed several times with distilled water until disappearance of chloride. The resulting iron hydroxide was dried at various temperatures between 110 and 300°C for 4 h. For the Fe_xO_y materials, Fe_xO_y-A stands for the samples prepared with $Fe(NO_3)_3$, Fe_xO_y-B stands for the samples prepared with $FeCl_2$, and Fe_xO_y-C stands for the samples prepared with $FeCl_3$.

Characterization

The catalysts were characterized by N_2-sorption, powder X-ray diffraction (XRD), transmission electron microscopy (TEM) and X-ray photoelectron spectroscopy (XPS).

N_2-sorption

N_2-sorption isotherms were measured at −197°C using a Micromeritics ASAP 2010. Prior to the experiments, the samples were dehydrated at 100°C until the vacuum pressure was below 5 μm Hg. The measurement of the surface areas of the samples was achieved by Brunauerr-Emmett-Teller (BET) method for relative pressures in the range $P/P_0 = 0.05 - 0.2$.

XRD

The XRD experiments were performed using a Siemens D500 powder diffractometer. The XRD patterns were collected using $CuK\alpha_1$ radiation (0.15405 nm) at a voltage and current of 40 kV and 30 mA, respectively. The sample was scanned over the range 20–80° 2θ at a rate of 0.05°/min to identify the crystalline structure. Sample for XRD were prepared as thin layers on a sample holder.

TEM

The morphologies and particle sizes of the samples were determined by TEM on a JEM-1200 EX II operated at 160 kV. Initially, a small amount of sample was put into the sample tube filled with a 95% ethanol solution. After agitating under ultrasonic environment for 10 min, one drop of the dispersed slurry was dipped onto a carbon coated copper mesh (300#) (Ted Pella Inc., CA, USA), and dried in an oven at 100°C for 1 h. Images were recorded digitally with a Gatan slow scan camera (GIF).

XPS

The XPS spectra were recorded with a Thermo VG Scientific Sigma Prob spectrometer. The XPS patterns were collected using AlKα radiation at a voltage and current of 20 kV and 30 mA, respectively. The base pressure in the analyzing chamber was maintained on the order of 10^{-9} torr. The spectrometer was operated 23.5 eV pass energy. The binding energy of XPS were corrected by contaminant carbon ($C_{1s} = 285.0$ eV) in order to facilitate the comparisons of the values among the catalysts and the standard compounds.

CO oxidation reaction

Catalytic activity was measured using a fixed bed continuous-flow reactor. A sample was placed in a pyrex glass tube, No treatment was applied before the measurements of catalytic activity. Catalyst sample was loaded into the reactor. The reactant gas (1 vol. % CO and 0.603 vol.% H_2O in air) was admitted with various flow rates through the reactor. Moisture was added to the reactant gas by using wet molecular sieves and a water bubbler. The moisture concentration was monitored by electric capacitance dew-point hygrometers. The flow rates were controlled by mass flow controllers. The carbon monoxide concentrations were monitored in the effluent gas while the reaction temperature was increased linearly from ambient to 160°C at the rate of 2°C /min. No treatment was applied before the measurements of catalytic activity. The temperature of catalyst bed was measured by a thermocouple placed inside the catalysts bed. Quantitative analysis of CO and CO_2 was performed by a gas chromatography with TCD using argon as the carrier gas. A CO analyzer (Industrial Scientific Corp., model T82) was used to analyze the CO concentration in the effluent down to 1 ppm.

The CO conversion was calculated based on the CO consumption as follows:

$$\%\ \text{of conversion of CO} = \frac{[\text{CO}]_{\text{in}} - [\text{CO}]_{\text{out}}}{[\text{CO}]_{\text{in}}} \times 100 \quad (1)$$

Results and discussion

Surface area

The samples all showed brown colored, free flowing powder. The surface areas of the Fe_xO_y materials prepared in this study are summarized in Table 1. In this study, the effects of preparation parameters, such as the precursor of iron, feeding rate of aqueous solution of iron salt, pH value, drying temperature, and drying time, on the properties of Fe_xO_y materials have been investigated. Table 1 shows that the surface areas of these materials are in the wide range between 20 and 406 m^2/g. The surface area increased from 20 to 406 m^2/g upon using $FeCl_3$ as the starting material. The results show clearly that only $FeCl_3$ allowed one to obtain the Fe_xO_y with high surface area. The surface area decreased in the order of Fe_xO_y-C > Fe_xO_y-A > Fe_xO_y-B. Besides, as the drying time for the Fe_xO_y support was more than

Table 1. Effect of preparation parameters on the surface areas of iron oxide

Iron salt	pH	Calcination temperature (°C)	Calcination time (h)	Surface area (m^2/g)
$Fe(NO_3)_3$	8	250	12	41
$Fe(NO_3)_3$	9	200	12	71
$Fe(NO_3)_3$	9	250	12	47
$Fe(NO_3)_3$	10	300	12	49
$Fe(NO_3)_3$	10	190	4	30
$FeCl_2$	9	110	1	20
$FeCl_2$	9	150	4	20
$FeCl_2$	9	180	4	22
$FeCl_2$	9	190	4	21
$FeCl_2$	10	110	1	24
$FeCl_2$	10	110	8	25
$FeCl_2$	10	130	4	20
$FeCl_2$	10	150	4	21
$FeCl_2$	10	180	4	25
$FeCl_2$	10	180	4	34
$FeCl_2$	10	110	1	49
$FeCl_2$	11	110	4	89
$FeCl_2$	11	110	8	90
$FeCl_3$	9	120	12	326
$FeCl_3$	9	180	4	312
$FeCl_3$	10	120	12	333
$FeCl_3$	10	180	4	276
$FeCl_3$	11	120	12	406
$FeCl_3$	11	180	4	336
$FeCl_3$	12	120	12	365
$FeCl_3$	12	180	4	346

4 h, the surface area did not change with increasing drying time, indicating that 4 h calcination time is long enough.

The surface areas of the Fe_xO_y-C materials synthesized at various pH values and dried at various temperatures are shown in Figure 1. The maximum surface area was obtained at pH 11. The surface area of Fe_xO_y-C decreased with an increase of drying temperature. It demonstrates that careful selection of pH value and drying temperature are the key points to have high surface area of Fe_xO_y materials. It also demonstrates that the surface area of Fe_xO_y-C was greater than 400 m^2/g with careful control the preparation parameters. The Fe_xO_y-C obtained by precipitation at pH 11 and dried at 120°C gave the largest surface area (406 $m^2\ g^{-1}$). In our knowledge, this is the highest surface area of iron oxide reported in the literature. Kozlova et al. (1998) used $Fe(NO_3)_3$ and Na_2CO_3 to prepare the iron oxide samples. $Fe(NO_3)_3$ was added dropwise (8 ml/min) to an aqueous solution of Na_2CO_3 under vigorous stirring. Final pH of the mixture was ca. 9.1. They showed that specially prepared iron oxide possesses about 10 times larger surface area. However, the highest surface area was only 195 m^2/g. Neri et al. (1998) reported iron oxide samples by addition of a solution of $Fe(NO_3)_3$ to an aqueous solution of Na_2CO_3 1 M (pH 11.9) or NaOH 1 M (pH 14) under vigorous stirring (500 rpm) at 7.5 ml/min rate and at temperature at 0 and 75°C. The surface area was in the range of 1–195 m^2/g. Venugopal and Scurrell (2004) used $Fe(NO_3)_3$ and NH_4OH to prepare iron hydroxide. The highest surface area they obtained was only 54 m^2/g.

XRD

XRD of the Fe_xO_y-A

The XRD patterns of the Fe_xO_y-A synthesized at various pH values and heated at 190°C are show in Figure 2. The XRD patterns of the Fe_xO_y-A samples exposed only wide, without any definite XRD peaks, suggesting that the material was either amorphous or of a particle size too small (< 40 nm). Li et al. (2003) reported that the

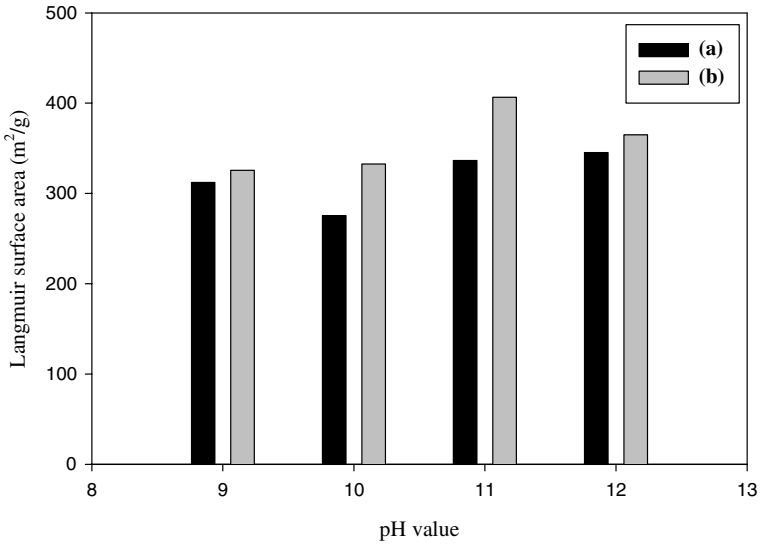

Figure 1. The surface areas of the Fe_xO_y-C synthesized at various pH values and dried at (a) 120°C and (b) 180°C.

powder XRD patterns of Fe_2O_3 nanoparticle (2–5 nm) catalysts revealed only broad, indistinct reflections, suggesting that the material was either amorphous or of a particle size too small for this method to resolve, in accordance with the results in this study.

XRD of the Fe_xO_y-B

The XRD patterns of the Fe_xO_y-B synthesized at pH value of 10 and dried at various temperatures are shown in Figure 3. Diffraction peaks of crystalline phase were compared with those of standard compounds reported in the JCPDS data file.

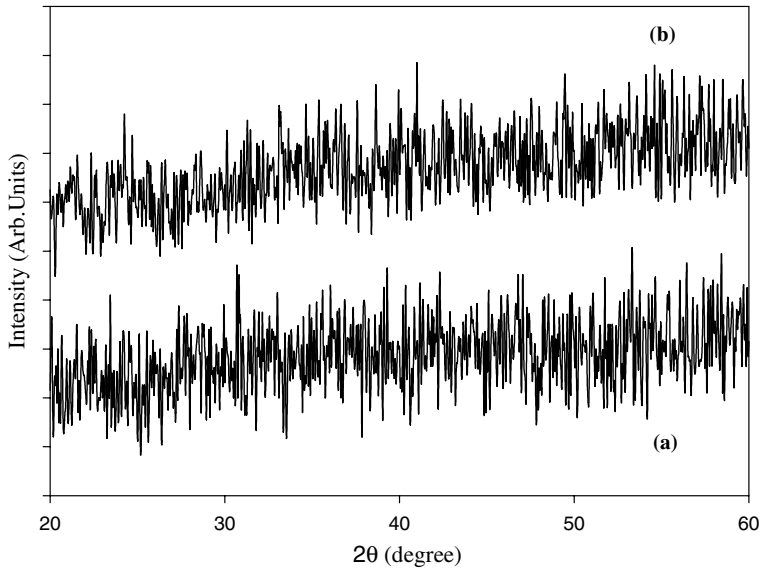

Figure 2. Effect of pH value of synthesis mixture on the crystalline phase of Fe_xO_y-A (a) pH 7 and (b) pH 10. The Fe_xO_y-A was prepared by precipitation method using NH_4OH and $Fe(NO_3)_3$ and dried at 190°C.

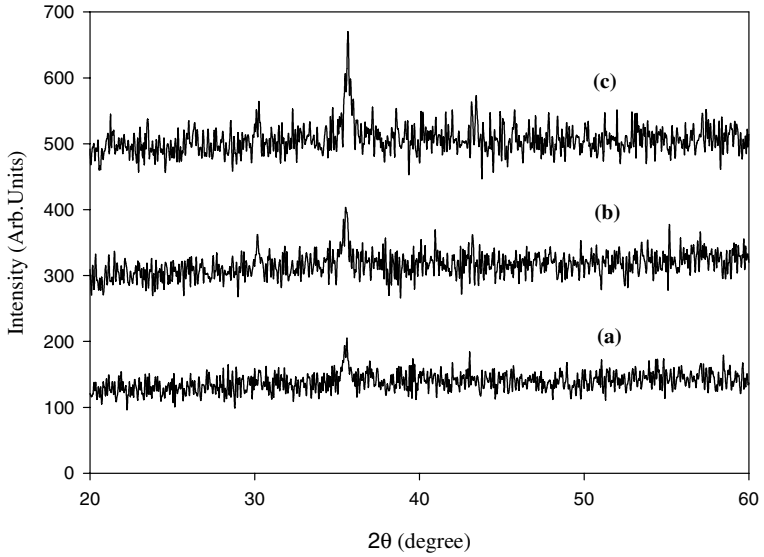

Figure 3. Effect of drying temperature on the crystalline phase of Fe_xO_y-B (a) 110°C, (b) 130°C, and (c) 150°C. The Fe_xO_y-B was prepared by precipitation method using NH_4OH and $FeCl_2$ and synthesized at pH 10.

According to this file, the XRD patterns in Figure 3 are similar to the prevailing crystallographic phase of magnetite ($FeFe_2O_4$). These patterns also show that magnetite ($FeFe_2O_4$) $\rightarrow$ maghemite (γ-Fe_2O_3) transition occurs at a temperature above 150°C because the intensities of the peaks ($2\theta = 30.335°$ and $43.4228°$) increased with an increase in the calcination temperature.

XRD patterns of the Fe_xO_y -C

The XRD patterns of the Fe_xO_y-C catalysts synthesized at various pH values and heated at

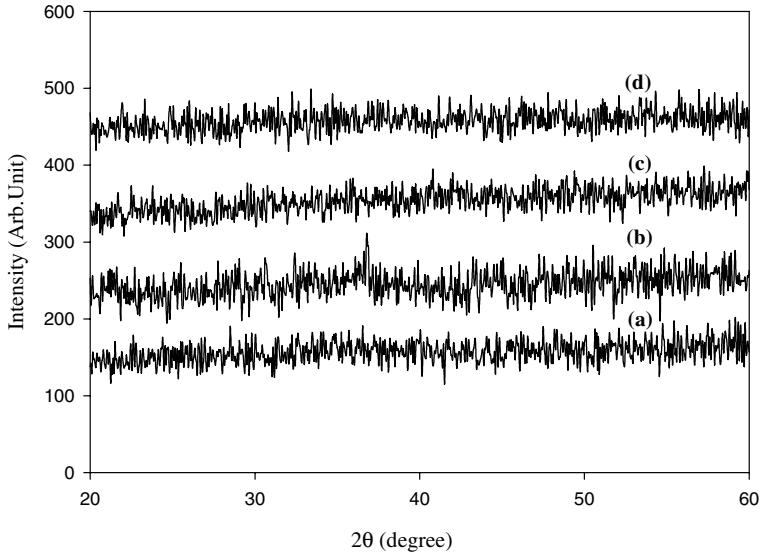

Figure 4. Effect of pH value on the crystalline phase of Fe_xO_y-C(a) pH 9, (b) pH 10, (c) pH 11 and (d) pH 12. The Fe_xO_y-C was prepared by precipitation method using NH_4OH and $FeCl_3$ and heated at 120°C.

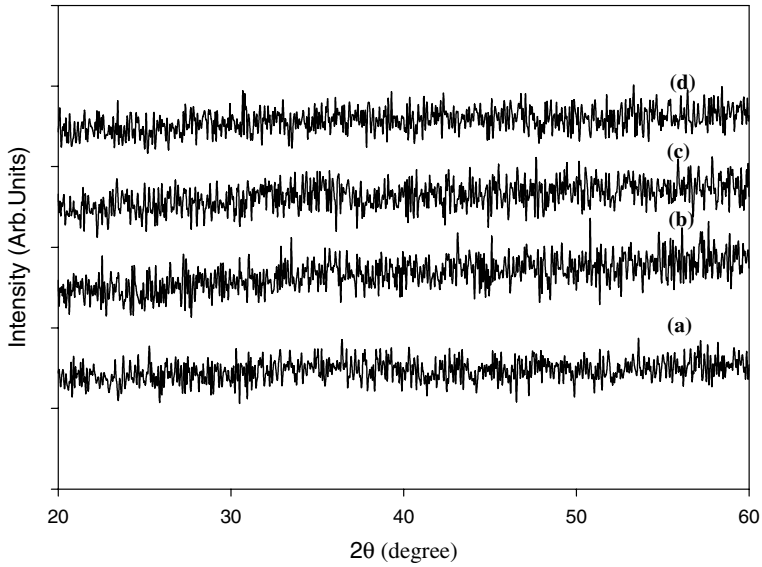

Figure 5. Effect of pH value on the crystalline phase of Fe_xO_y-C (a) pH 9, (b) pH 10, (c) pH 11 and (d) pH 12. The Fe_xO_y-C was prepared by precipitation method using NH_4OH and $FeCl_3$ and heated at 180°C.

various temperatures are shown in Figures 4, 5 and 6. Figure 4 shows that the samples dried at 120°C presents a XRD pattern without distinct peaks, indicating a completely amorphous structure. Heating the Fe_xO_y-C sample at 180°C did not cause any modifications in the XRD pattern as shown in Fig. 5. Both Figures 4 and 5 appear amorphous structures, due to their low heating temperature. On the contrary, when the samples were heated at 300°C, the XRD patterns (Figure 6) started to show multiple peaks with low intensities. The peak intensities of the XRD peaks of the Fe_xO_y-C samples were strongly dependent on the heating temperature, the intensity increased with increasing

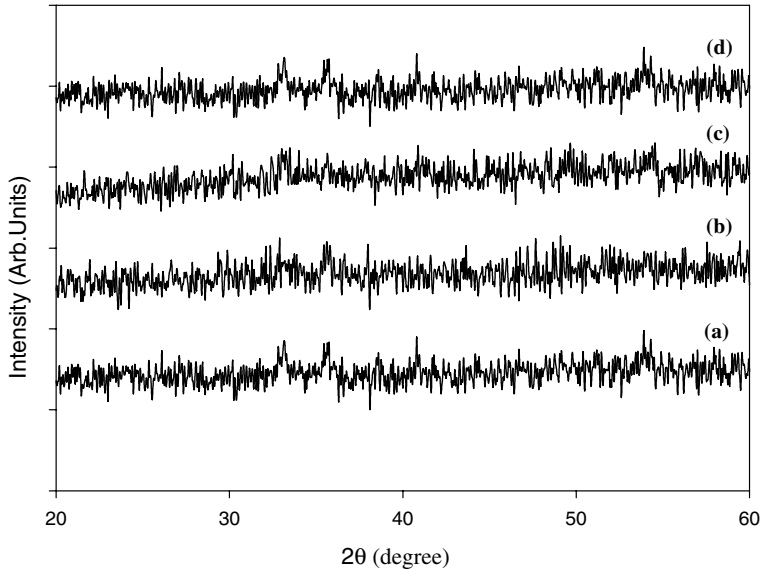

Figure 6. Effect of pH value on the crystalline phase of Fe_xO_y-C (a) pH 9, (b) pH 10, (c) pH 11 and (d) pH 12. The Fe_xO_y-C was prepared by precipitation method using NH_4OH and $FeCl_3$ and heated at 300°C.

the heating temperature, as expected. Nevertheless, the material was amorphous as long as the pretreatment temperature was less than 200°C.

The crystalline phases were different for the Fe_xO_y-C samples treated with various heating temperatures. According to the JCPDS data file, Figure 6 shows that the Fe_xO_y-C heated at 300°C gave the diffraction peaks of hematite (α-Fe_2O_3). This is in agreement with the results of Liaw et al. (1989) who have reported that peaks of minor intensity, related to crystalline hematite, were found after the thermal treatment and attributed to the transition goethite $\rightarrow$ hematite which is known to occur at above 250°C. Neri et al. (1999) also showed that hematite (α-Fe_2O_3) is the prevailing crystallographic phase of Fe_2O_3, in accordance with the results of this study.

XRD patterns of iron oxides prepared with various precursors

For the iron oxide samples, the XRD analysis showed the presence of different crystalline iron oxide (hydroxides) phases. According to the above results, one can conclude that Fe_xO_y-A and Fe_xO_y-C showed amorphous pattern for low-temperature treated samples (< 200°C). It also demonstrated that $FeCl_3$ is more preferable than $FeCl_2$ to have the Fe_xO_y with high surface area and amorphous structure. The Fe_xO_y-C showed a surface area (> 300 m^2 g^{-1}) with an amorphous structure (see Table 2) by appropriate preparation conditions.

TEM

TEM of the Fe_xO_y-B

Figure 7 shows the particle size of the Fe_xO_y-B as a function of pH value (9, 10 and 11) after heating at 120°C. For the sample synthesized at pH 9, as shown in Figure 7a, the particle size of Fe_xO_y-B was very large, having diameter of greater than 30 nm. Controlling the pH values at 10 during the synthesis of Fe_xO_y-B samples gave a smaller particle size with a diameter of 10 nm as shown in Figure 7b. These results demonstrate that the material synthesized at pH 10 gave the smallest particle size for the sample Fe_xO_y-B. The pH value during precipitation plays an important role.

Figure 8 shows the particle size of the Fe_xO_y-B samples synthesized at pH 9 and 10 and dried at 180°C, respectively. The feeding rates were varied from 20 to 80 ml/min. From these photos, one can see that the particle size of the Fe_xO_y-B sample is strongly dependent on the feeding rate of the starting materials. The particle size of the Fe_xO_y-B decreased with decreasing the feeding rate of the starting material. This is in agreement with the results of Cunningham et al. (1998) who have reported that to control the size distribution a saturated solution of magnesium citrate was added slowly to the aqueous dispersion over a period of between 10 min to 1 h. The fast addition over 10-min periods typically gives rise to larger final size distributions upon calcinations. Kozlova et al. (1998) and Neri et al. (1999) also used very low feeding rates to prepare the nanosized iron oxide. However, they did not report the effect of feeding rate on the size of iron oxide.

The TEM images of the Fe_xO_y-C

The TEM images of the Fe_xO_y-C synthesized at various pH values and feeding rates of the starting materials and heated at various temperatures are shown in Figures 9, 10 and 11. Both Figures 9 and 11 show that the smaller Fe_xO_y-C particles with the size less than 5 nm were prepared at a feeding rate of 10 ml/min. The large Fe_xO_y-C particles (shown in Figure 10) with the size between 20 and 35 nm were pre-

Table 2. Characteristics of the Fe_xO_y-C samples

Sample	Crystalline phase	S.A. (m^2/g)
Fe_xO_y-C synthesized at pH 9 and dried at 120°C	Amorphous	326
Fe_xO_y-C synthesized at pH 9 and dried at 180°C	Amorphous	312
Fe_xO_y-C synthesized at pH 10 and dried at 120°C	Amorphous	333
Fe_xO_y-C synthesized at pH 10 and dried at 180°C	Amorphous	275
Fe_xO_y-C synthesized at pH 11 and dried at 120°C	Amorphous	345
Fe_xO_y-C synthesized at pH 11 and dried at 180°C	Amorphous	345
Fe_xO_y-C synthesized at pH 12 and dried at 120°C	Amorphous	345
Fe_xO_y-C synthesized at pH 12 and dried at 180°C	Amorphous	345

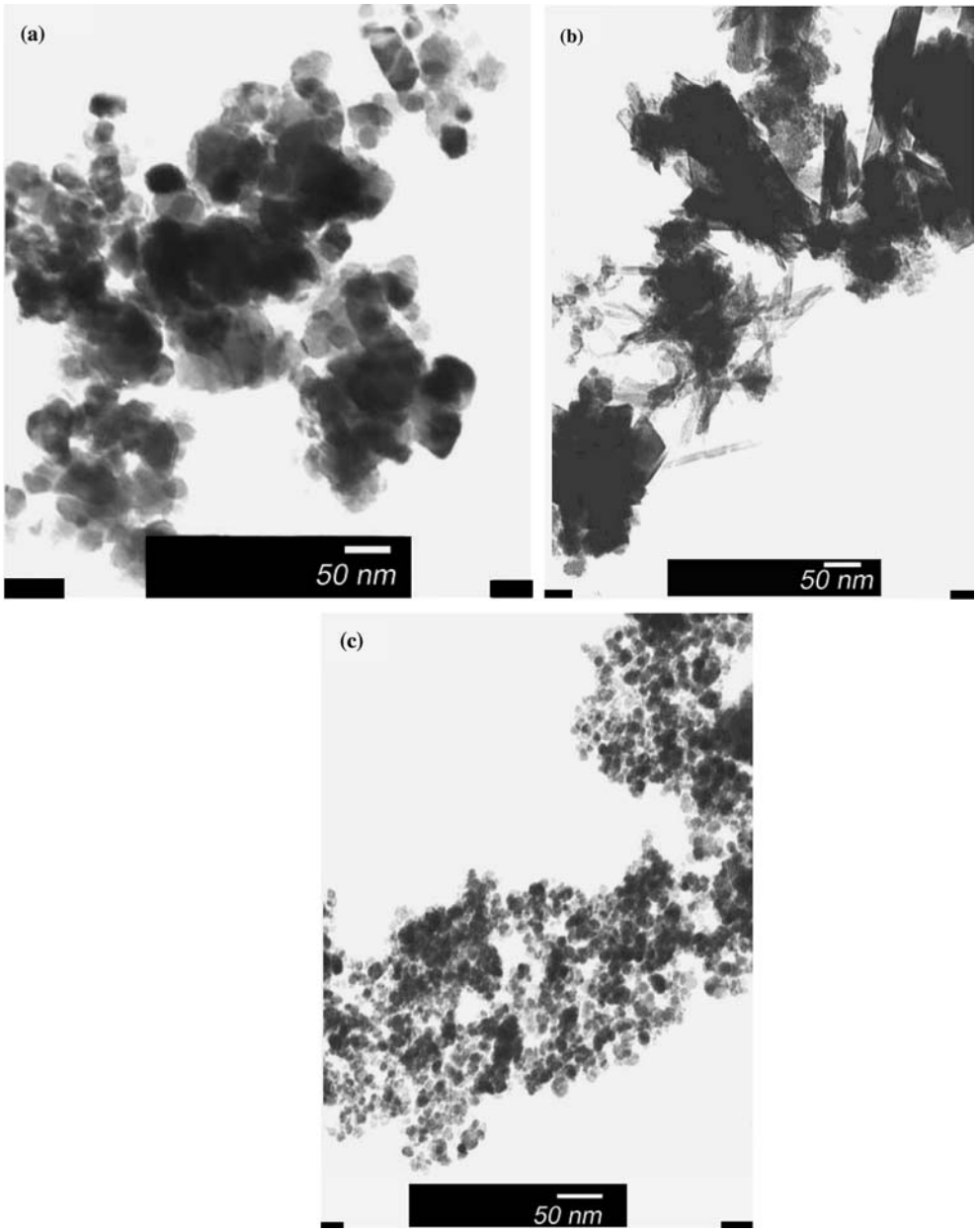

Figure 7. Effect of pH value on the TEM images of Fe_xO_y-B (a) pH 9, (b) pH 10, (c) pH 11. The Fe_xO_y-B was prepared by precipitation method using NH_4OH and $FeCl_2$ and heated at 120°C.

pared at a feeding rate of 30 ml/min. One can conclude that the feeding rate of the aqueous solution of the starting material is an important factor to control particle size of iron oxide. Under the same pH value and heating temperature, the particle size of Fe_xO_y-C decreased with decreasing feeding rate of iron precursor. In addition, the size distribution became narrower upon decreasing the feeding rate. In order to control the particle size and size distribution, the solutions of the iron precursor should be fed slowly to the aqueous medium.

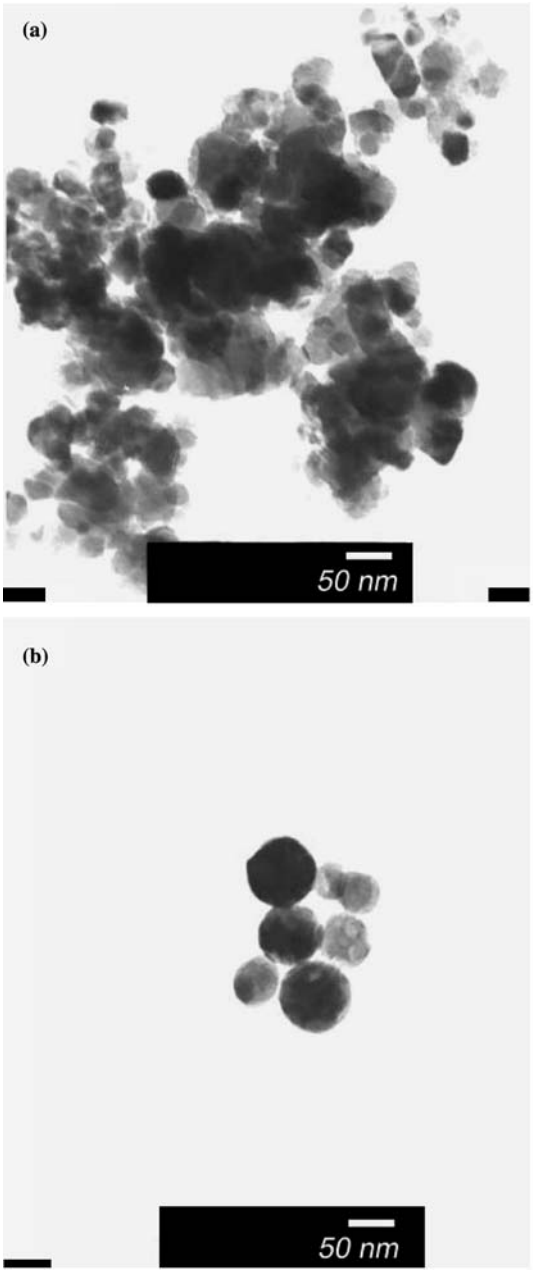

Figure 8. Effect of pH value on the TEM images of Fe_xO_y-B (a) pH 9, (b) pH 10. The Fe_xO_y-B was prepared by precipitation method using NH_4OH and $FeCl_2$ and heated at 180°C.

The Fe_xO_y-C materials showed a particle size of less than 5 nm, in accordance with an amorphous structure and high surface areas (see Table 3). One can conclude that the materials prepared with $FeCl_3$,

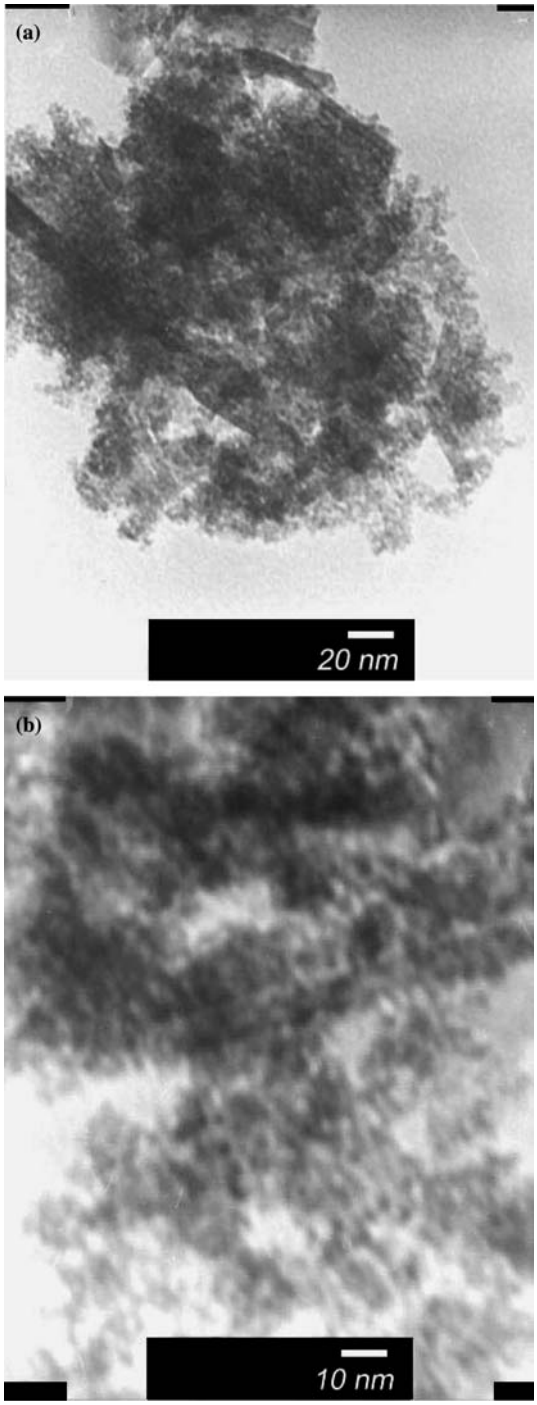

Figure 9. Effect of drying temperature on the TEM images of the Fe_xO_y-C samples, (a) 120°C, (b) 180°C. The Fe_xO_y-C was prepared by precipitation method using NH_4OH and $FeCl_3$ and at pH 10.

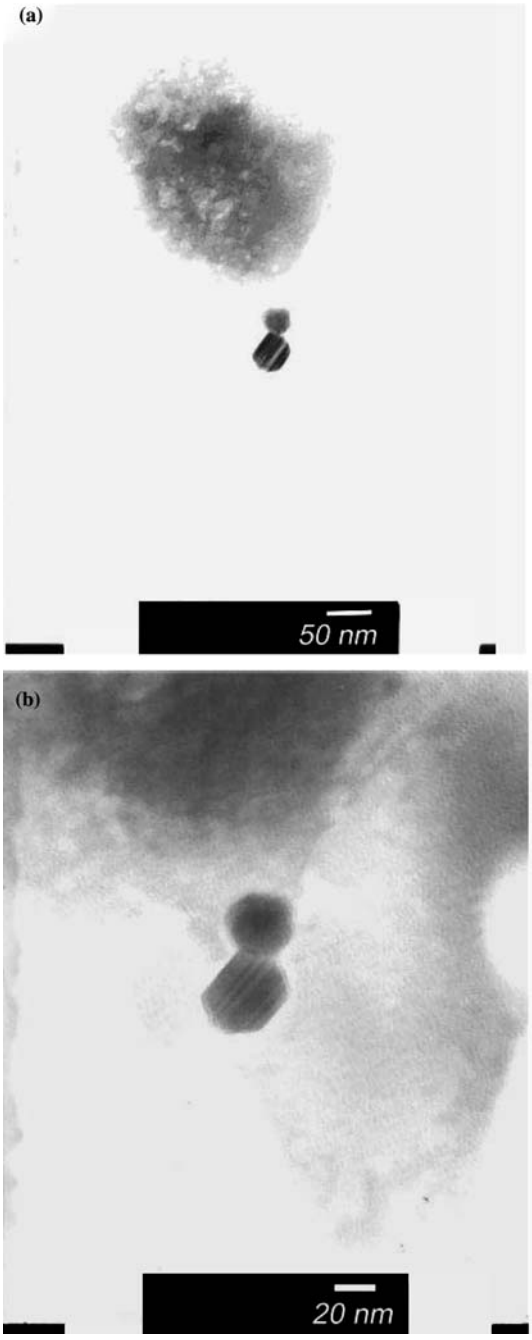

Figure 10. The TEM images of FexOy-C dried at 180°C. The Fe_xO_y was prepared by precipitation method using $FeCl_3$ and synthesized at pH 10.

low feeding rate, pH 11, and low heating temperature (< 200°C) gave a high surface area, small particle size and amorphous structure of iron oxides.

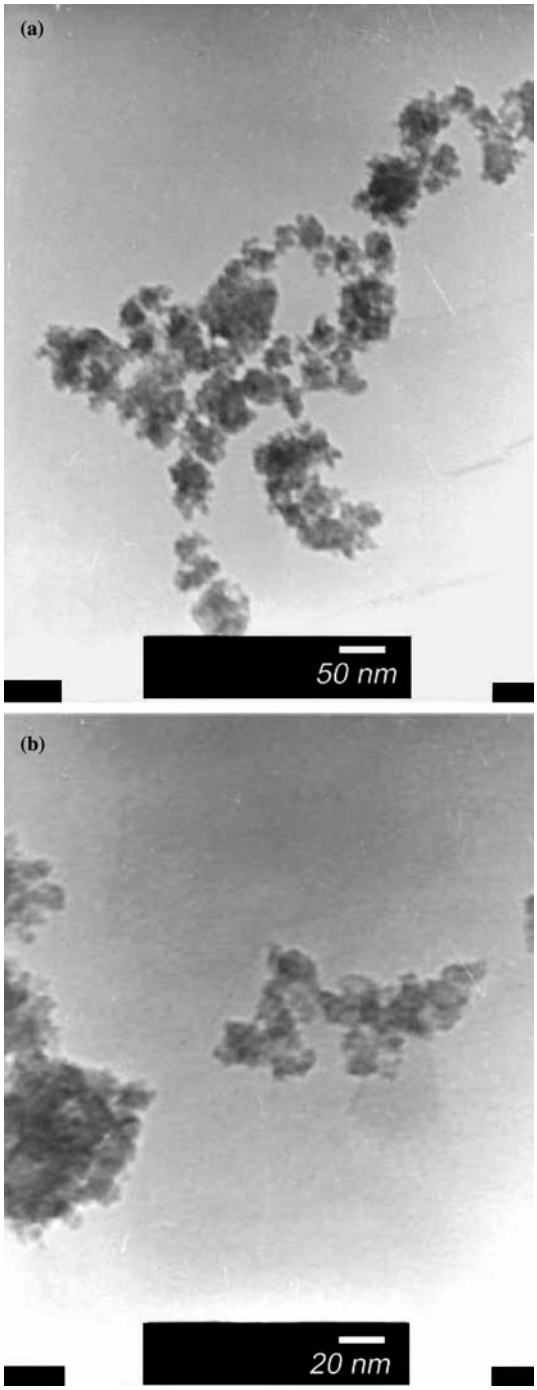

Figure 11. Effect of drying temperature of Fe_xO_y-C samples on the TEM images, (a) 120°C, and (b) 180°C. The Fe_xO_y-C was prepared by precipitation method using NH_4OH and $FeCl_3$ and synthesized at pH 11.

Table 3. Characteristics of the Fe_xO_y-C samples

Sample	pH in the synthesis mixture	Drying temperature (°C)	Surface area (m^2/g)	crystalline phase	particle diameter
Fe_xO_y-C	10	120	333	Amorphous	<4 nm
Fe_xO_y-C	10	180	275	Amorphous	<4 nm
Fe_xO_y-C	11	120	406	Amorphous	<4 nm
Fe_xO_y-C	11	180	336	Amorphous	<4 nm

XPS

XPS was employed to obtain information of the surface state of iron oxide. XPS Fe 2p spectra of the Fe_xO_y-C sample heated at 120°C and synthesized at various pH values are given in Figure 12. The binding energies of Fe 2p is tabulated in Table 4. The binding energies were calibrated taking, as a reference, the adventitious C 1s peak at 285.0 eV. Table 4 shows the decreasing binding energy (BE) of Fe $2p_{1/2}$ with increasing pH value of the synthesis mixture. The Fe_xO_y-C synthesized at pH value of 8 had a higher BE of Fe $2p_{3/2}$ (711.2 eV) than the other Fe_xO_y-C samples (710 eV) synthesized at pH of 9, 10, 11 and 12, respectively. According to the standard XPS binding energy (eV) of Fe $2p_{3/2}$, the Fe $2p_{3/2}$ and satellite peaks for Fe_xO_y-C (pH 8) were observed at 711.4 and 719.6 eV, which are close to those for Fe_3O_4. The XPS spectra (Figure 12) of the Fe_xO_y samples prepared at pH of 9, 10, 11 and 12, respectively, showed the Fe $2p_{3/2}$ peaks around 710 eV. A shake-satellite peak is between 717 and 719 eV for all samples. According to the standard XPS binding energy of Fe $2p_{3/2}$, XPS Fe $2p_{3/2}$ spectra showed the phase transition of iron from Fe_3O_4 to FeO with increasing pH. The Fe $2p_{3/2}$ peaks, therefore, corresponds probably to two kinds of iron oxide species, which can be correlated with small particles as observed in TEM images. Horvath et al. (2000) reported that the binding energy of Fe 2p appeared between 710.8 and 710.5 eV, which shows the presence of Fe_2O_3 and/or FeO(OH) species. Kozlova et al. (1998) reported that the shift of the XPS Fe $2p_{3/2}$ peak for $Fe(OH)_3$ sample to 710.8 eV, which is an indication of the formation of mixed-valence oxide Fe_3O_4. Various researchers also reached the same conclusions (Brundle et al., 1977; Kuivila et al., 1988; Epling et al., 1996).

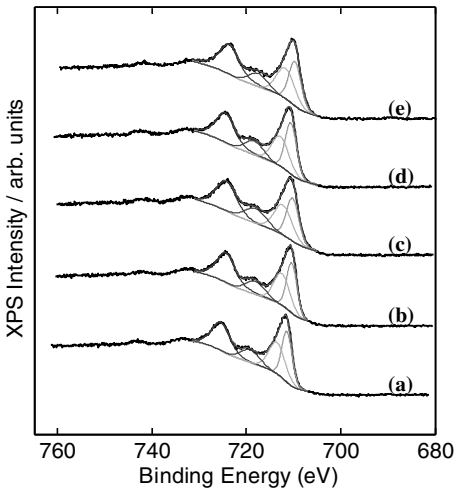

Figure 12. Effect of pH value on the XPS Fe 2p spectra of Fe_xO_y-C (a) pH 8, (b) pH 9, (c) pH 10, (d) pH 11, (e) pH 12. The Fe_xO_y was prepared by precipitation method using NH_4OH and $FeCl_3$-C and dried at 120°C.

CO oxidation on Fe_xO_yCatalysts

The catalytic activities of the Fe_xO_y samples for CO oxidation are shown in Figure 13. The reactant gas was 0.25 vol.% CO and 6031 ppm moisture in air. The carbon monoxide concentrations were monitored in the effluent gas while the reaction temperature was increased linearly from ambient to 160°C at the rate of 2°C/min.

Generally, the CO oxidation over metal oxides can be broken down into two steps:

$$MO + CO = M + CO_2 \quad (2)$$

$$M + \frac{1}{2}O_2 = MO \quad (3)$$

where M is the metal.

The catalytic CO oxidation is exothermic. Li et al. (2003) reported that the first step of the catalytic reaction is for MO to lose one oxygen atom to carbon monoxide to form carbon dioxide.

Table 4. Effect of pH in the synthesis mixture on the XPS Fe 2p spectra of Fe_xO_y-C

Sample	XPS	
	$2p_{1/2}$(eV)	$2p_{3/2}$(eV)
Fe_xO_y-C synthesized at pH 8 and dried at 120°C	725.3	711.2
Fe_xO_y-C synthesized at pH 9 amd dried at 120°C	724.5	710.3
Fe_xO_y-C synthesized at pH 10 and dried at 120°C	724.0	710.1
Fe_xO_y-C synthesized at pH 11 and dried at 120°C	724.5	710.4
Fe_xO_y-C synthesized at pH 12 and dried at 120°C	723.3	709.9

The Fe_xO_y-C was prepared by precipitation method using NH_4OH and $FeCl_3$

The tendency of MO to lose one oxygen atom to carbon monoxide should be an important factor in determining how good a catalyst MO is.

The effectiveness of Fe_xO_y power as a catalyst for CO oxidation is obvious, as shown in Figure 13, the conversion of CO as a function of reaction temperature for Fe_xO_y-C with a surface area of 406 m^2/g, exposed to the 0.25 vol.% CO and 0.603 vol.% H_2O in air. The space-velocity was 30,106 km/h. In the case of Fe_xO_y-C (surface area = 406 m^2/g), with a steady rise in reaction temperature, it was observed that 37% conversion of CO was obtained at room temperature and 60% conversion was obtained at 100°C. This catalyst was very active compared to the data reported by Li et al. (2003). It appeared plausible to suggest that the Fe_xO_y-C provided high carbon monoxide conversion efficiency. It is to be noted that the iron oxide sample in this study had good catalytic activity at ambient condition for CO oxidation. This property is important in many useful applications. The previous liertaure have shown that iron oxide was only active at temperature above 180°C.

Li et al. (2003) reported the effectiveness of NANOCAT® over the non-nano Fe_2O_3 powder as a catalyst for CO oxidation. An amount of 50 mg of the NANOCAT® can catalyze oxidation of almost 100% of the carbon monoxide to carbon dioxide at 350°C in an inlet gas mixture of 3.44% carbon monoxide and 20.6% oxygen at 1000 ml/min. Under identical conditions, the same amount of the α-Fe_2O_3 powder with a particle size of 5 m, can only catalyze oxidation of less than 5% of the

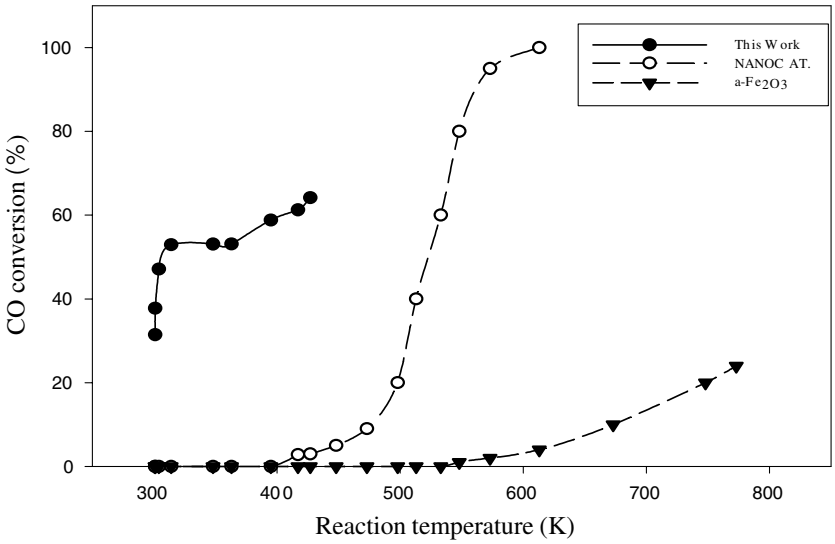

Figure 13. CO conversion on Fe_xO_y-C compared with the literature data.ion method using NH_4OH and $Fe(NO_3)_3$ and heated at 190°C.

carbon monoxide to carbon dioxide. It should be noted that CO was not converted at room temperature in their study (Li et al. 2003). However, the space velocity they used was greater than that in this study. In a parallel study, we have tested our catalyst at the same space velocity as Li et al. (2003), 15% CO conversion was obtained. In the literature, no one has reported the iron oxide catalyst which had CO conversion at room temperature. Li et al. (2003) reported the higher activity of Fe_2O_3 nanoparticles over non-nano Fe_2O_3 powders for CO oxidation only at temperature above 210°C. It was attributed to a small size (3 nm) and the presence of an hydroxylated phase of iron oxide (FeOOH). However, iron oxide nanoparticles are only active at 210°C. Kozlova et al. (1998) used $Fe(NO_3)_3$ and Na_2CO_3 to prepare the iron oxide samples. The iron oxide was active for CO oxidation only at temperature higher than 190°C. The high activity of Fe_xO_y nanoparticles prepared in this study was attributed to a small particle size, high surface area, more hydroxyl groups, and more densely populated surface coordination unsaturated sites.

Conclusion

In this study, we present a method to prepare iron oxide material which has a higher surface area and nanosized particle. It was used as a catalyst for CO oxidation at low temperature. The preparation conditions had significant effect on the characteristics of Fe_xO_y. The iron oxide prepared by the precipitation at pH 11 using $FeCl_3$ with low feeding rate (10 ml/min), followed by washing 20 times at least with distilled water until disappearance of chloride, then dried in a flow of air at a temperature below 180°C gave the smallest particle size and the highest surface area (>400 m^2/g), small and uniform particle size (3 nm) and amorphous structure of iron oxide. However, large amount of hydroxyl groups were preserved if the drying temperature was below 200°C The XRD patterns of the iron oxide samples prepared with $FeCl_3$, heated at a temperature below 180°C appeared only wide, without any definite XRD peaks, suggesting that the material was either amorphous or of a particle size too small (<4 nm) to be detected. The broad peak appeared XRD patterns of the iron oxide samples prepared by different conditions showed the phase transition of the iron oxide samples from amorphous to various crystalline phases were depending on the preparation conditions. The XPS Fe $2p_{3/2}$ spectra showed the Fe_3O_4 and FeO mixed oxide phases. The catalysts were test in the conditions with the reactant gas of 0.25 vol. % CO and 0.603 vol. % H_2O in air, space-velocity of 30,106 km/h and the pretreatment temperature of 180°C. For the Fe_xO_y sample with surface area of 406 m^2/g, 37% conversion of CO was obtained at room temperature. The higher activity of Fe_xO_y nanoparticles developed in this study was attributed to a small particle size, high surface area, more hydroxyl groups, and more densely populated surface coordination unsaturated sites.

Acknowledgements

The authors would like to express thanks to the Ministry of Economic Affairs, Taiwan, Republic of China, for their support of the advanced scientific research under contract number 92-EC-17-A09-S1–022.

References

Avgouropoulos G., T. Ioannides, C. Papadopoulou, J. Batista, S. Hocevar & H.K. Matralis, 2002. A comparative study of Pt/gamma -Al_2O_3, Au/alpha-Fe_2O_3 and CuO–CeO_2 catalysts for the selective oxidation of carbon monoxide in excess hydrogen. Catal. Today 75, 157–167.

Bond G.C. & D.T. Thompson, 1999. Catalysis by gold. Catal. Rev. Sci Eng. 41, 319–388.

Brundle C.R., T.J. Chuang & K. Wandelt, 1977. Core and valence level photoemission studies of iron oxide surfaces and the oxidation of iron. Surf. Sci. 68, 459–468.

Cameron D., C. Corti, R. Holliday & D. Thompson, 2003. Gold-based catalysts for hydrogen processing and fuel cell systems. adapted from web site of world Gold Council, http://www.wgc.org.

Epling W.S., G.B. Hoflund & J.F. Weaver, 1996. Surface characterization study of Au/α-Fe_2O_3 and Au/Co_3O_4 low-temperature CO oxidation catalysts. J. Phys. Chem. 100, 9929–9934.

Feng Z., J. Zhao, F.E. Huggins & G.P. Huffman, 1993. Agglomeration and phase transition of a nanophase iron oxide catalyst. J. Catal. 143, 510–519.

Haruta M., 2004. Nanoparticulate gold catalysts for low-temperature CO oxidation. J. N. Mater. Electrochem. Syst. 7, 163–172.

Huffman G.P., B. Ganguly, J. Zhao, K.R.P.M. Rao, N. Shah, Z. Feng, F.E. Huggins, M.M. Taghiei, F. Lu, I. Wender, V.R. Pradhan, J.W. Tierney, M.S. Seehra, M.M. Ibrahim, J. Shabtai & E.M. Eyring, 1993. Structure and dispersion of Fe-based catalysts for direct coal liquefaction. Energy Fuels 7, 285–296.

Kozlova A.P., A.I. Kozlov, S. Sugiyama, Y. Matsui, K. Asakura & Y. Iwasawa, 1999. Study of gold species in iron-oxide-supported gold catalysts derived from gold-phosphine complex $Au(PPh_3)(NO_3)$ and as-precipitated wet $Fe(OH)_3$. J. Catal. 181, 37–48.

Kuivila C.S., J.B. Butt & P.C. Stair, 1988. Characterization of surface species on iron synthesis catalysts by X-ray photoelectron spectroscopy. Appl. Surf. Sci. 32, 99–121.

Li P., D.E. Miser, S. Rabiei, T.T. Yadav & M.R. Hajaligol, 2003. The removal of carbon monoxide by iron oxide nanoparticles. Appl. Catal. B 43, 151–162.

Tabakova T., V. Idakiev, D. Andreeva & I. Mitov, 2000. Influence of the microscopic properties of the support on the catalytic activity of Au/ZnO, Au/ZrO_2, Au/Fe_2O_3, Au/Fe_2O_3–ZnO, Au/Fe_2O_3–ZrO_2 catalysts for the WGS reaction. Appl. Catal. A 202, 91–97.

Venugopal A. & M.S. Scurrell, 2004. Low temperature reductive pretreatment of Au/Fe_2O_3 catalysts, TPR/TPO studies and behaviour in the water-gas shift reaction. Appl. Catal. A 258, 241–249.

Wu K.C., Y.L. Tung, Y.L. Chen & Y.W. Chen, 2004. Catalytic oxidation of carbon monoxide over gold/iron hydroxide catalyst at ambient conditions. Appl. Catal. B 53, 111–116.

Zhao J., F.E. Huggins, Z. Feng, F. Lu, N. Shah & G.P. Huffman, 1993. Structure of a nanophase iron oxide catalyst. J. Catal. 143, 499–509.